Amending entanglement-breaking channels via intermediate unitary operations

Á. Cuevas,[1] A. De Pasquale,[2] A. Mari,[2] A. Orieux,[1,3,4] S. Duranti,[1,5] M. Massaro,[1,6] A. Di Carli,[1,7] E. Roccia,[1,8] J. Ferraz,[1,9] F. Sciarrino,[1] P. Mataloni,[1] and V. Giovannetti[2]

[1]*Dipartimento di Fisica, Università di Roma La Sapienza, 00185 Rome, Italy*
[2]*NEST, Scuola Normale Superiore, and Istituto Nanoscienze CNR, 56127 Pisa, Italy*
[3]*LIP6, CNRS, Université Pierre et Marie Curie, Sorbonne Universités, 75005 Paris, France*
[4]*IRIF, CNRS, Université Paris Diderot, Sorbonne Paris Cité, 75013 Paris, France*
[5]*Dipartimento di Fisica e Geologia, Università degli Studi di Perugia, 06123 Perugia, Italy*
[6]*Department of Physics, University of Paderborn, 33098 Paderborn, Germany*
[7]*Department of Physics, University of Strathclyde, Scottish Universities Physics Alliance, Glasgow G4 0NG, United Kingdom*
[8]*Dipartimento di Fisica, Università degli Studi Roma Tre, 00146 Rome, Italy*
[9]*Departamento de Física, Universidade Federal Rural de Pernambuco, 52171-900 Recife, Brazil*

(Received 1 July 2017; published 23 August 2017)

We report a bulk optics experiment demonstrating the possibility of restoring the entanglement distribution through noisy quantum channels by inserting a suitable unitary operation (filter) in the middle of the transmission process. We focus on two relevant classes of single-qubit channels consisting in repeated applications of rotated phase-damping or rotated amplitude-damping maps, both modeling the combined Hamiltonian and dissipative dynamics of the polarization state of single photons. Our results show that interposing a unitary filter between two noisy channels can significantly improve entanglement transmission. This proof-of-principle demonstration could be generalized to many other physical scenarios where entanglement-breaking communication lines may be amended by unitary filters.

DOI: 10.1103/PhysRevA.96.022322

I. INTRODUCTION

Real quantum communication channels are typically not perfect transmission lines, since they usually introduce different kinds of noises given by the intrinsic mechanisms that transfer information or by external perturbations. Physically, such channels disturb the transmitted messages by gradually degrading the information along their structures [1–3] and this effect may be particularly severe when entangled qubits are propagated through them. The extreme limit is represented by entanglement-breaking (EB) channels [4] that are so noisy to be useless for an entanglement distribution even exploiting distillation techniques [5], with direct consequences on the associated classical or quantum capacities [6].

In many practical situations, quantum channels can be represented as the consecutive application of a given elementary map Φ repeated n times, where n is a positive integer. In this cases, the full channel is given by

$$\Phi^n = \underbrace{\Phi \circ \Phi \circ \cdots \circ \Phi}_{n \text{ times}} \tag{1}$$

and the integer n can be interpreted as the effective length of the transmission line. For example, if the elementary map Φ corresponds to the spatial propagation of a quantum state along a physical medium of length l, then the total length of the channel is nl. Alternatively, if Φ models the dissipative evolution of the system lasting an elementary time interval τ, then $n\tau$ represents the total time duration of the whole process. In these cases one may ask what is the maximum entanglement propagation length or, equivalently, what is the minimum $n = k$ such that Φ^k is EB. Such a number k can be seen as a sort of noise quantifier for the elementary map Φ and corresponds to its entanglement-breaking order originally defined in [7] and further investigated in [8–10].

In this work we give an experimental proof-of-principle demonstration that the propagation length can be increased by placing intermediate unitary operations (filters) between the elementary maps Φ. More precisely, we implement two different examples [built up by exploiting single-qubit phase-damping (PD) and amplitude-damping (AD) channels, respectively] of an elementary map Φ of $k = 2$ such that

$$\Phi \circ \Phi \text{ is EB}, \tag{2}$$

while, for a suitable unitary operation $\mathcal{F}$,

$$\Phi \circ \mathcal{F} \circ \Phi \text{ is not EB}. \tag{3}$$

In practice, the action of the filter $\mathcal{F}$ is to "amend" the otherwise EB communication line, by properly acting in the middle of the transmission process. Therefore, the length of the channel up to which quantum correlations are preserved is increased. Together with the recent results reported in Ref. [10] in which dissipative correcting operations have been considered, the present work represents an experimental demonstration of such an entanglement recovery technique.

From a theoretical perspective this idea was already introduced in [7], where it was also shown that for some maps Φ (including those considered in the next section) the entanglement propagation length can be increased from $k - 1$ to an arbitrary number q of repetitions, i.e., one can have

$$\underbrace{\Phi \circ \mathcal{F} \circ \Phi \circ \cdots \circ \mathcal{F} \circ \Phi}_{q \text{ times}} \text{ is not EB}. \tag{4}$$

In this work, however, we consider only the case of $q = k = 2$ iterations represented in Eq. (3) for two main reasons: in the first place, our main motivation is to present a proof of concept as simple as possible of this recovery effect and, secondly, experimental entanglement transmission for many iterations

$q \gg 2$ is quite hard to achieve due to unavoidable technical imperfections of the associated large-scale experiments. For these reasons our method must not be considered as competitive or superior to standard quantum communication schemes based on quantum repeaters. Our results are instead complementary to such techniques: for example, one could use our methods to increase the distance between two repeaters of a quantum network or to amend quantum channels in which repeaters are difficult to implement for technical reasons (e.g., in long undersea optical fibers).

The paper is organized as follows. In Sec. II we present the idea and the theoretical model of the two experiments: the first one based on rotated phase-damping maps and the second one based on rotated amplitude-damping maps. In Sec. III we present all the details of the experimental implementation. In Sec. IV we report and discuss the experimental results. Eventually, in Sec. V we draw some conclusions.

II. THEORETICAL MODEL OF THE EXPERIMENT

In this section we present the two experimental schemes that we used to verify the unitary filtering phenomenon compactly summarized by Eqs. (2) and (3). For both experiments we focused on single-qubit channels acting on the polarization state of individual photons. The vertical and horizontal polarizations of the photon form a basis $\{|V\rangle,|H\rangle\}$ of a two-dimensional Hilbert space. In this basis, a generic quantum state can be expressed as a 2×2 density matrix $\rho \in \mathbb{C}^2$ such that $\rho \geqslant 0$ and $\mathrm{Tr}[\rho] = 1$.

As real candidates for the elementary map Φ appearing in Eq. (2), we considered the rotated phase-damping and the rotated amplitude-damping maps, respectively given by the following composition of operations:

$$\Phi_{\mathrm{PD}} = \Lambda_{\pi/8} \circ \Gamma, \tag{5}$$

$$\Phi_{\mathrm{AD}} = \Lambda_{\pi/4} \circ \Sigma, \tag{6}$$

where $\Lambda_{\pi/8}$ and $\Lambda_{\pi/4}$ are unitary rotations defined by

$$\Lambda_\theta(\rho) = R_\theta \rho R_\theta, \quad R_\theta = \begin{pmatrix} \cos(2\theta) & -\sin(2\theta) \\ -\sin(2\theta) & -\cos(2\theta) \end{pmatrix}, \tag{7}$$

Γ is the phase-damping channel [11,12] with damping parameter $p \in [0,1]$,

$$\Gamma(\rho) = \left(1 - \frac{p}{2}\right)\rho + \frac{p}{2}\sigma_z \rho \sigma_z, \quad \sigma_z = R_{\theta=0}, \tag{8}$$

and Σ is the amplitude-damping channel [11,12] with the parameter $\eta \in [0,1]$,

$$\Sigma(\rho) = E_1 \rho E_1^\dagger + E_2 \rho E_2^\dagger, \tag{9}$$

with $E_1 = \left(\begin{smallmatrix} 1 & 0 \\ 0 & \sqrt{1-\eta} \end{smallmatrix}\right)$ and $E_2 = \left(\begin{smallmatrix} 0 & \sqrt{\eta} \\ 0 & 0 \end{smallmatrix}\right)$. In both cases ($\Phi = \Phi_{\mathrm{PD}}$ and $\Phi = \Phi_{\mathrm{AD}}$), as a potential candidate for the generic unitary filter appearing in (3) we use

$$\mathcal{F} = \Lambda_\varphi, \tag{10}$$

where φ is an angle that we are going to optimize and Λ_φ is a unitary operation defined analogously to Λ_θ as in Eq. (7). Our aim is to experimentally verify that there exist values or intervals of the damping parameters p or η and of the filter angle φ such that both conditions (2) and (3) are fulfilled, demonstrating that the unitary filter succeeds in increasing the entanglement propagation distance.

Before presenting the details of the experimental implementation, we anticipate here how the previous three maps (7)–(9) can be realized using standard bulk optics elements such as beam splitters and phase plates, and how one can experimentally test whether a given sequence of maps is entanglement breaking or not. The implementation of the unitary rotation Λ_φ is very simple since it corresponds to the application of a $\lambda/2$ phase plate rotated by an angle φ around the propagation axis of the photon. The phase-damping channel (8) can also be implemented quite easily as a probabilistic switch between the identity operation $\mathbb{I}$ and the map σ_z. The application of the amplitude-damping channel (9) to a polarization qubit is instead less straightforward but can still be simulated with a suitable interferometric scheme as explained in the next section. Finally, we recall that, in order to test whether a channel is entanglement breaking or not, it is sufficient to apply it to a subsystem of a maximally entangled state and check the separability of the output state [4]:

$$\Phi \text{ is EB} \iff (\Phi \otimes I)|\Psi\rangle_{sa}\langle\Psi| \text{ is separable}, \tag{11}$$

where I is the identity map on an arbitrary ancillary system a and $|\Psi\rangle_{sa}$ is a maximally entangled state of the bipartite system composed by the considered system s and a.

III. EXPERIMENTAL IMPLEMENTATION

Our experimental scheme adopts a Sagnac interferometric source of polarization-entangled photons [13] in a Bell state $|\Psi\rangle_{sa} = \frac{1}{\sqrt{2}}(|0\rangle_s|1\rangle_a + e^{i\phi}|1\rangle_s|0\rangle_a)$, $|0\rangle \equiv |H\rangle$ ($|1\rangle \equiv |V\rangle$) being the horizontal (vertical) polarization. The photons are generated in two indistinguishable type-II parametric down-conversion processes inside a periodically poled potassium titanyl phosphate (PPKTP) nonlinear crystal. Here the photons belonging to a continuous wave laser of 405 nm are converted into twin photons of 810 nm at a rate of 60 000 pairs/s and heralded efficiency of 16% revealed by two synchronized avalanche photodetectors (APDs). The high purity of the generated state was measured, giving a fidelity of $F_{\mathrm{exp}} = 0.980 \pm 0.016$ to $|\Psi\rangle_{sa}$ [14] and a concurrence of $C_{\mathrm{exp}} = 0.973 \pm 0.004$ [15]. In order to take into account the imperfect purity of the input entangled state, we can model it as a Werner state $\rho_W = \frac{4F-1}{3}\rho_{sa} + \frac{1-F}{3}\mathbb{I}_s \otimes \mathbb{I}_a$ [6,16], where $\mathbb{I}_x$ is the identity operator associated with subsystem x.

In order to test condition (11) in the laboratory, the s photon (i.e., the photon that embodies the system s) is injected in a bulk optics setup that implements $\Omega = \Phi \circ \Phi$ or $\Omega' = \Phi \circ \mathcal{F} \circ \Phi$, while the a photon (i.e., the ancillary system) propagates in free space. The bipartite output state ρ_{sa}^{out} is measured by a hypercomplete tomography setup [17] (see Fig. 1). Then the s and a photons are coupled into single-mode fibers (SMFs) directly connected to an APD. The setup allows to measure the degree of entanglement remaining after the action of each implemented map.

A. Rotating phase-damping channel

To simulate each Γ channel [Eq. (8)], two operations are needed, $\mathbb{I}$ and σ_z. They are simply implemented by the absence

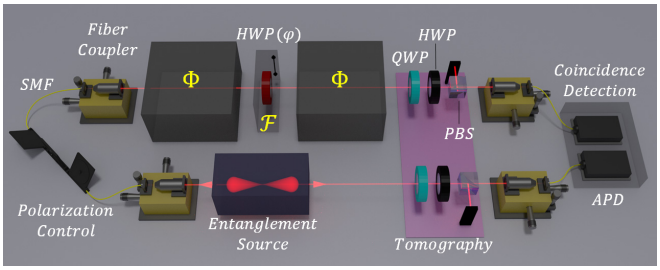

FIG. 1. Scheme of the experimental setup. A source of polarization entangled qubits sends the a photon directly to the tomography stage, while the s photon is transmitted by a SMF to the simulation of $\Omega = \Phi \circ \Phi$ or $\Omega' = \Phi \circ \mathcal{F} \circ \Phi$ and then measured in the same temporally synchronized bipartite tomography. The maps $\Phi = \Phi_{\mathrm{PD}}$ or $\Phi = \Phi_{\mathrm{AD}}$ are represented by the black boxes, while $\mathcal{F} = \Lambda_\varphi$ is represented by the transparent-gray box enclosing a half-wave plate HWP(φ). Finally, we specify that Ω (Ω') corresponds to the absence (presence) of HWP(φ).

or presence of a half-wave plate (HWP) fixed at 0° in the optical path of the photon, respectively. To simulate Λ_θ another HWP is permanently placed after Γ, but with a rotation degree of freedom in the angle θ [as shown in Fig. 2(a)] [6,18].

Since both Λ_θ plates are synchronized in their rotation angle, there are only four combinations of Pauli operations; when the first Φ_{PD} is applying $\mathbb{I}$, the second Φ_{PD} can apply $\mathbb{I}$ or σ_z; when the first Φ_{PD} is applying σ_z, the second Φ_{PD} can apply $\mathbb{I}$ or σ_z. Then the statistical mixture between $\mathbb{I}$ and σ_z is obtained by extracting a fraction $P_{\mathbb{I}\mathbb{I}} = (1 - \frac{p}{2})^2$ of coincidences from the $\mathbb{I} + \mathbb{I}$ tomography, a fraction $P_{\mathbb{I}\sigma_z} = (1 - \frac{p}{2})\frac{p}{2}$ of coincidences from the $\mathbb{I} + \sigma_z$ and $\sigma_z + \mathbb{I}$ tomographies, and a fraction $P_{\sigma_z\sigma_z} = (\frac{p}{2})^2$ from the $\sigma_z + \sigma_z$ tomography. Once the tomography registry fractions are combined, the new registry will be equivalent to a tomography of the state under the action of $\Omega_{\mathrm{PD}} = \Phi_{\mathrm{PD}} \circ \Phi_{\mathrm{PD}}$.

B. Rotating amplitude-damping channel

To simulate each Σ channel, we use a displaced Sagnac interferometer (SI), opened and closed by a single polarizing beam splitter (PBS) [as shown in Fig. 2(b)]. The parallel trajectories of $|V\rangle$ and $|H\rangle$ projections inside the SI are temporally compensated and go in the clockwise and counterclockwise directions, respectively. Both trajectories are intercepted by

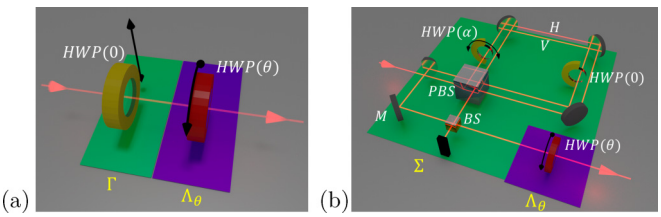

FIG. 2. Single-channel modules. (a) Plot of Φ_{PD}: The unrotated yellow plate HWP(0) constitutes the PD channel Γ, since $\mathbb{I}$ is applied when it is absent or σ_z when it is present. (b) Plot of Φ_{AD}: The SI and MZI constitute the AD channel Σ, transforming the vertical polarization into horizontal by a rotation of HWP(α). In both (a) and (b), the rotating red plate HWP(θ) represents Λ_θ.

independent HWPs: a rotating one, HWP(α), for $|V\rangle$ and another unrotated one, HWP(0), for $|H\rangle$. The rotation angle α is related to the damping parameter η by the expression $\alpha(\eta) = \frac{\arccos(-\sqrt{1-\eta})}{2}$ [6,10].

After the SI there is an unbalanced Mach-Zehnder interferometer (MZI) that allows to couple in the same trajectory the damped and undamped polarizations as they pass through a beam splitter (BS). The temporal difference between the MZI arms is set to a value larger than the coherence length of the photons in order to simulate random-phase fluctuations that destroy quantum interferences at its output. The action of $\Omega_{\mathrm{AD}} = \Phi_{\mathrm{AD}} \circ \Phi_{\mathrm{AD}}$ is then obtained by selecting the same damping η in both Σ, while both HWPs corresponding to Λ_φ rotate in a synchronous way.

C. Filtering

The protocol first requires us to fix the damping parameter p for Ω_{PD} or η for Ω_{AD} to scan the channel in the rotation angle θ and verify the location of periodic EB regions. It results that these regions are located around $\theta_{\mathrm{PD}} = \frac{\pi}{8} \pm n\frac{\pi}{4}$ for the $(\Omega_{\mathrm{PD},s} \otimes \mathbb{I}_a)(\rho_{sa})$ experiment and around $\theta_{\mathrm{AP}} = \frac{\pi}{4} \pm n\frac{\pi}{2}$ for the $(\Omega_{\mathrm{AD},s} \otimes \mathbb{I}_a)(\rho_{sa})$ experiment, in both cases with $n \in \mathbb{N}$. Once this condition is experimentally certified, one proceeds to fix the angle $\theta = \theta_{\mathrm{PD}}$ or $\theta = \theta_{\mathrm{AD}}$. Then the operation of $\mathcal{F}$ is studied by scanning the rotation φ of an extra HWP (as shown in Fig. 1). As a consequence, either $\Omega'_{\mathrm{PD}} = \Phi_{\mathrm{PD}} \circ \Lambda_\varphi \circ \Phi_{\mathrm{PD}}$ or $\Omega'_{\mathrm{AD}} = \Phi_{\mathrm{AD}} \circ \Lambda_\varphi \circ \Phi_{\mathrm{AD}}$ will no longer be EB in a region where Ω_{PD} and Ω_{AD} are EB.

IV. RESULTS

In Fig. 3 we report the experimental results for the channels Ω_{PD} and Ω'_{PD} acting over the s photon of a pair of entangled photons, with the damping parameter set to the value $p = 0.65$. Figure 3(a) shows the EB behavior of Ω_{PD} around $\theta_{\mathrm{PD}} = \pm\frac{\pi}{8}$ as predicted by the simulated model, while Fig. 3(b) shows an entanglement revival of Ω'_{PD} for $\varphi = \pm\frac{\pi}{8}$. Similarly, in Fig. 4 we report the results of Ω_{AD} and Ω'_{AD} channels acting over the s photon from a pair of entangled photons, having set the damping parameter to the value $\eta = 0.66 \pm 0.017$. Figure 4(a) shows the EB behavior of Ω_{AD} around $\theta_{\mathrm{AD}} = \pm\frac{\pi}{8}$ as predicted by the simulated model, while Fig. 4(b) shows an entanglement revival of Ω'_{AD} for $\varphi = \frac{\pi}{8}$.

The experimental data were obtained by averaging and calculating the standard deviation over five values per point. The blue lines were calculated by considering perfect input state and optical conditions. The simulated shaded green areas correspond to the regions of all possible experimental results within one standard deviation of $F_{\mathrm{exp}} = 0.980 \pm 0.016$ for Ω_{PD} and Ω'_{PD} and also consider the error propagation of 0.5° of uncertainty in θ for Ω_{AD} and Ω'_{AD}. This difference in the data analysis between PD and AD channels originates from the negligible error contribution of 0.5° of uncertainty in PD channels. All $C_{\mathrm{exp}} = 0$ values have error bars within the size of the point.

The simulated data considered two scenarios: one with perfect optical elements (POEs) and a maximally pure entangled input state, and another with realistic optical elements (ROEs), a nonmaximally pure entangled input state, and error

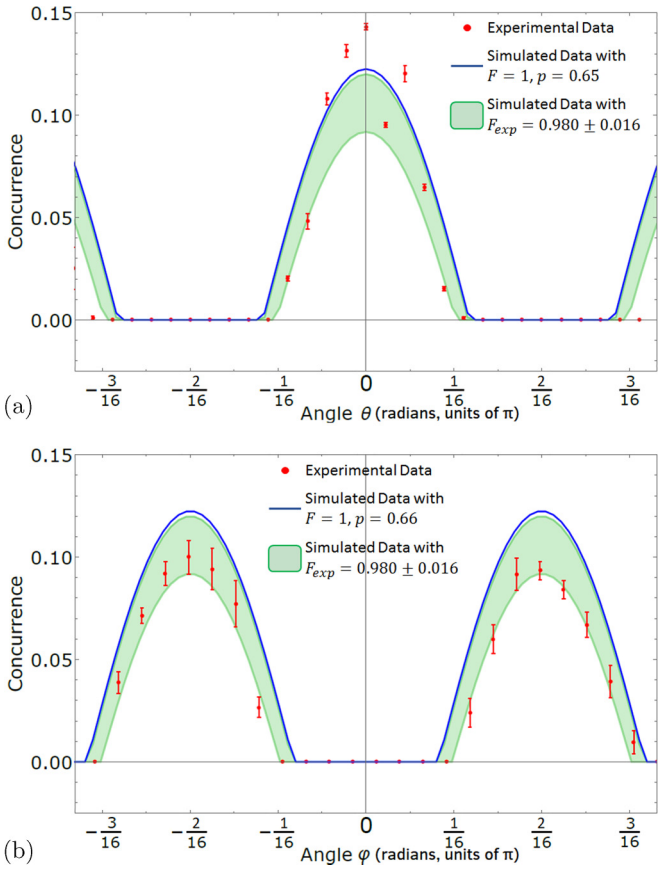

FIG. 3. Concurrence vs PD mapping for $p = 0.65$. Red points represent the experimental data. Blue lines represent the simulated data for perfect optical elements and a pure entangled state with $F = 1$. Green shaded areas represent the regions of simulated data for realistic optical elements and a mixed entangled state within one standard deviation of the fidelity $F_{\text{exp}} = 0.980 \pm 0.016$. (a) Plot of Ω_{PD}, obtained by rotating θ, with EB behavior around $\theta = \pm\frac{\pi}{8}$. (b) Plot of Ω'_{PD}, obtained by rotating φ, with a revival of entanglement around $\varphi = \pm\frac{\pi}{8}$, while θ is fixed at $\frac{\pi}{8}$.

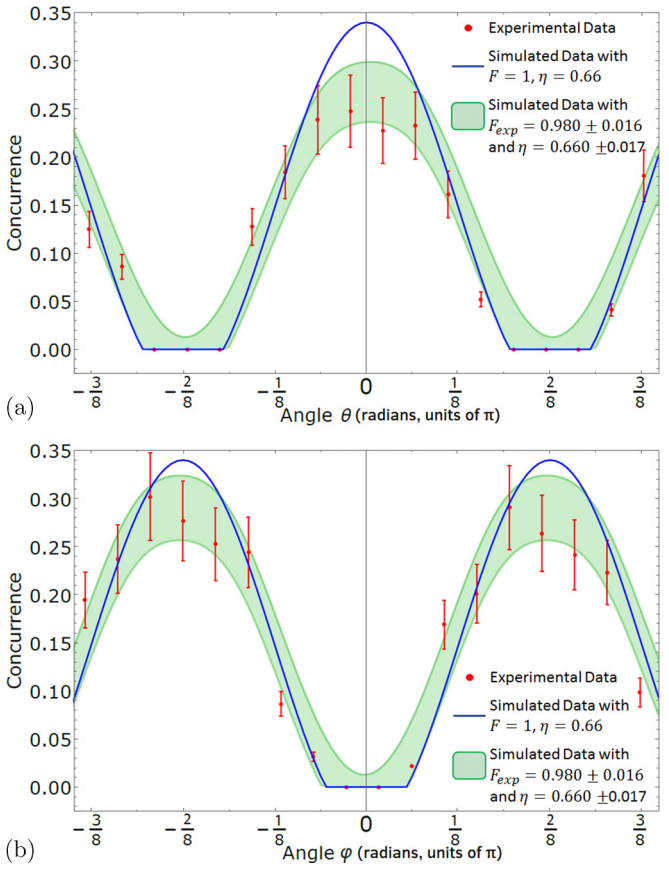

FIG. 4. Concurrence vs AD mapping for $\eta = 0.66$. Red points represent the experimental data. Blue lines represent the simulated data for perfect optical elements and a pure entangled state with $F = 1$. Green shaded areas represent the regions of simulated data for realistic optical elements and a mixed entangled state within one standard deviation of the fidelity $F_{\text{expt}} = 0.980 \pm 0.016$ and the propagated error of the damping $\eta = 0.66 \pm 0.017$. (a) Plot of Ω_{AD}, obtained by rotating θ, with EB behavior around $\theta = \pm\frac{\pi}{4}$. (b) Plot of Ω'_{AD}, obtained by rotating φ, with a revival of entanglement around $\varphi = \pm\frac{\pi}{4}$, while θ is fixed at $\frac{\pi}{4}$.

propagation. The differences between these two cases are described in Table I.

In both PD (Fig. 3) and AD (Fig. 4) cases there is a good agreement between experimental and simulated data.

TABLE I. Optical parameters and state fidelities. The acronyms TH and TV represent the transmissivities in the horizontal and vertical polarizations, respectively; RH and RV represent the reflectivities in the horizontal and vertical polarizations, respectively.

Parameter	POE	Average ROE
Fidelity (F)	1	0.980 ± 0.016
TH_{BS}	0.5	0.507 ± 0.016
RH_{BS}	0.5	0.407 ± 0.011
TV_{BS}	0.5	0.495 ± 0.018
RV_{BS}	0.5	0.410 ± 0.001
TH_{PBS}	1	0.965 ± 0.001
RH_{PBS}	0	0.008 ± 0.004
TV_{PBS}	0	0.024 ± 0.014
RV_{PBS}	1	0.928 ± 0.035

The discrepancies existing between Ω_{PD} and Ω'_{PD} and their simulations could be attributed to the postprocessing generation of the channel, since their action has been simulated by combining $\mathbb{I}$ and σ_z operations with unstable photon counts during long-time scans varying θ and φ rotation angles. On the other hand, discrepancies between Ω_{AD} and Ω'_{AD} and their simulations are strongly related to the difficulty of coupling the 16 possible spatial modes within a unique SMF at the end of the entire channel.

Our results constitute an experimental validation of the entanglement recovery effect summarized by Eqs. (2) and (3). As discussed in the Introduction, the iteration of the same filtering method beyond two repetitions ($q > 2$) of the map Φ is theoretically possible, however, the practical implementations present technical difficulties depending on the kind of channels under study. In the cases considered in this work, for q-filtered Φ_{PD} channels, their concatenation must be temporally synchronized to correctly apply 2^q possible operations. For q-filtered Φ_{AD} channels, all the 4^q spatial modes must be correctly collected by a single SMF. As a

consequence, a large number of filtered iterations represents a challenging experimental task beyond the aim of this work.

V. CONCLUSION

We have given an experimental proof for a method aiming at increasing the entanglement transmission distance, applicable to communication lines decomposable into elementary maps. The technique consists in placing appropriate unitary operations between the elementary steps of the channel, allowing one to restore the entanglement transmissivity of an initially entanglement-breaking communication line.

We implemented different single-qubit channels acting on the polarization of single photons combining standard bulk optics elements: rotated phase plates, beam splitters and photodetectors. We applied such channels to a subsystem of a maximally entangled state and computed the remaining fraction of entanglement after performing a two-photon state tomography. We measured clear revivals of the output entanglement whenever a unitary filter, consisting of a phase plate with appropriate rotation angle, was placed in the middle of the transmission process. Our results could be extended to more general physical scenarios involving different single-qubit operations [7], continuous and nonunitary channels [10], or amendable Gaussian maps [8].

ACKNOWLEDGMENTS

Á.C. is grateful for the support from the Chilean agency Comisión Nacional de Investigación Científica y Tecnológica (CONICYT) and its Ph.D. scholarships program Becas Chile. J.F. is grateful for the support from the Brazilian agency Coordenação de Aperfeiçoamento de Pessoal de Nível Superior (CAPES) and the Ciência sem Fronteiras (CsF) program.

[1] H. Barnum, M. A. Nielsen, and B. Schumacher, Phys. Rev. A **57**, 4153 (1998).
[2] B. W. Schumacher, Phys. Rev. A **54**, 2614 (1996).
[3] I. L. Chuang and M. A. Nielsen, J. Mod. Opt. **44**, 2455 (1997).
[4] M. Horodecki, P. W. Shor, and M. B. Ruskai, Rev. Math. Phys. **15**, 629 (2003).
[5] C. H. Bennett, G. Brassard, S. Popescu, B. Schumacher, J. A. Smolin, and W. K. Wootters, Phys. Rev. Lett. **76**, 722 (1996).
[6] Á. Cuevas, M. Proietti, M. A. Ciampini, S. Duranti, P. Mataloni, M. Sacchi, and C. Macchiavello, Phys Rev. Lett. (to be published).
[7] A. De Pasquale and V. Giovannetti, Phys. Rev. A **86**, 052302 (2012).
[8] A. De Pasquale, A. Mari, A. Porzio, and V. Giovannetti, Phys. Rev. A **87**, 062307 (2013).
[9] L. Lami and V. Giovannetti, J. Math. Phys. **56**, 092201 (2015).
[10] Á. Cuevas, A. Mari, A. De Pasquale, A. Orieux, M. Massaro, F. Sciarrino, P. Mataloni, and V. Giovannetti, Phys. Rev. A **96**, 012314 (2017).
[11] M. A. Nielsen and I. L. Chuang, *Quantum Computation and Quantum Information* (Cambridge University Press, Cambridge, 2010).
[12] E. Desurvire, *Classical and Quantum Information Theory: An Introduction for the Telecom Scientist* (Cambridge University Press, Cambridge, 2009).
[13] A. Fedrizzi, T. Herbst, A. Poppe, T. Jennewein, and A. Zeilinger, Opt. Express **15**, 15377 (2007).
[14] R. Horodecki, P. Horodecki, M. Horodecki, and K. Horodecki, Rev. Mod. Phys. **81**, 865 (2009).
[15] W. K. Wootters, Phys. Rev. Lett. **80**, 2245 (1998).
[16] M. Barbieri, F. De Martini, G. Di Nepi, and P. Mataloni, Phys. Rev. Lett. **92**, 177901 (2004).
[17] D. F. V. James, P. G. Kwiat, W. J. Munro, and A. G. White, Phys. Rev. A **64**, 052312 (2001).
[18] A. Chiuri, V. Rosati, G. Vallone, S. Pádua, H. Imai, S. Giacomini, C. Macchiavello, and P. Mataloni, Phys. Rev. Lett. **107**, 253602 (2011).